# Rapid Evolution of Cool Season, Low-CAPE Severe Thunderstorm Environments

JESSICA R. KING, MATTHEW D. PARKER, KEITH D. SHERBURN, AND GARY M. LACKMANN

*Department of Marine, Earth, and Atmospheric Sciences, North Carolina State University, Raleigh, North Carolina*

(Manuscript received 1 August 2016, in final form 17 January 2017)

ABSTRACT

Low-CAPE (i.e., CAPE $\leq 1000\,\mathrm{J\,kg^{-1}}$) severe thunderstorms are common in the greater southeastern United States (including the Tennessee and Ohio valleys). These events are often poorly forecasted, and the environments in which they occur may rapidly evolve. Real-data simulations of 11 low-CAPE severe events and 6 low-CAPE nonsevere events were performed at convection-allowing resolution. Some amount of surface-based destabilization occurred during *all* simulated events over the 3-h period prior to convection. Most simulated severe events experienced comparatively large destabilization relative to the nonsevere events as a result of surface warming, cooling aloft, and surface moistening. The release of potential instability by large-scale forcing for ascent likely influenced the cooling aloft in some cases. Surface warming was attributable primarily to warm advection and appeared to be an important discriminator between severe and nonsevere simulated events. Severe events were also found to have larger low-level wind shear than nonsevere events, particularly during nocturnal cases. Because of the rapid destabilization that occurred within 3 h in the simulated events, it is evident that 3–6-hourly model output may not be adequate for forecasting severe events in high-shear, low-CAPE environments. Monitoring of high-resolution model forecasts and surface observations may be necessary to identify a rapidly changing severe environment.

## 1. Introduction

Severe and tornadic events in the United States predominantly occur in environments characterized by strong 0–6-km vertical wind shear and some amount of CAPE (Schneider and Dean 2008). Although strong shear is generally necessary for severe convection capable of producing thunderstorms and tornadoes, CAPE varies drastically among severe environments (Schneider et al. 2006; Schneider and Dean 2008; Grams et al. 2012). During the late spring and summer months, severe thunderstorms and tornadoes typically occur in environments with moderate-to-large amounts of CAPE (e.g., $>1000\,\mathrm{J\,kg^{-1}}$); however, during the late fall, winter, and early spring (herein referred to as the cool season), when CAPE is climatologically at its lowest, severe weather events can and do still occur (Guyer et al. 2006; Smith et al. 2008; Sherburn and Parker 2014). High-shear, low-CAPE,[1] hereafter HSLC, cool season severe weather events commonly take place during the late evening and overnight hours along the corridor from the Gulf Coast to the mid-Atlantic, including the Southeast and the Mississippi, Tennessee, and Ohio valleys (e.g., Guyer et al. 2006; Schneider et al. 2006; Schneider and Dean 2008; Smith et al. 2008; Thompson et al. 2008; Guyer and Dean 2010; Kis and Straka 2010; Coleman and Dixon 2014). The environments and structures of HSLC storms and their associated risks are reviewed in detail by Davis and Parker (2014) and Sherburn and Parker (2014).

Idealized modeling studies have tested the effects of different values of CAPE on storm structure and evolution. McCaul and Weisman (2001) initialized simulations with profiles having $800\,\mathrm{J\,kg^{-1}}$ bulk CAPE and found that these produced intense storms in the presence of large low-level shear, especially when CAPE was concentrated in the lowest levels of the profile. Kirkpatrick et al. (2011) found similar results, but also found that reducing CAPE below $800\,\mathrm{J\,kg^{-1}}$ increasingly inhibited strong updrafts and rotation. Jewett and Wilhelmson (2006) found that idealized simulations of environments with reduced CAPE and high shear did not produce intense, long-lasting convection in the absence of large-scale environmental forcing.

[1] Throughout the manuscript, HSLC refers to environments with SBCAPE $\leq 1000\,\mathrm{J\,kg^{-1}}$ and 0–3-km shear vector magnitude $\geq 18\,\mathrm{m\,s^{-1}}$. For simplicity, from here on we refer to a layer's bulk shear vector magnitude as shear, e.g., 0–3-km shear.

*Corresponding author e-mail*: Jessica King, jrking2@ncsu.edu

DOI: 10.1175/WAF-D-16-0141.1

TABLE 1. All simulated nonsevere events listed chronologically followed by all severe events listed chronologically. The case ID defines each case as a nonsevere event (NS) or a severe event (S) and its order chronologically among the nonsevere or severe events. Average end time is defined as the average end of the preconvective environment in the simulations, as described in section 2d. Location refers to states in which HSLC severe reports occurred. Maximum SPC outlook and SPC watch highlights the maximum risk within the HSLC location during convection in addition to any watches issued. SFCOA maximum SBCAPE (J kg$^{-1}$) refers to the maximum from the starting time to the ending time of the simulation. Average end-time (maximum) WRF SBCAPE (J kg$^{-1}$) is the average end-time CAPE for 49 points as described in section 2d. Average maximum WRF 0–3-km shear (m s$^{-1}$) refers to the average of the maximum 0–3-km shear for each of the 49 points throughout the simulated 3-h time series as described in section 2d.

| Case ID | Date | Avg simulated end time (LT) | Location of HSLC event | Max SPC outlook, SPC watch | SFCOA max SBCAPE (J kg$^{-1}$) | Avg end-time (max) WRF SBCAPE (J kg$^{-1}$) | Avg max WRF 0–3-km shear (m s$^{-1}$) |
|---|---|---|---|---|---|---|---|
| NS1 | 22 Dec 2007 | 1625 | AR, LA, MS, TN | Slight<br>Tornado | 140 | 299 | 27.6 |
| NS2 | 19–20 Mar 2008 | 2000 | NC, SC | Slight | 132 | 74 | 36.6 |
| NS3 | 28 Feb–1 Mar 2011 | 2215 | GA, FL | Slight<br>Severe thunderstorm | 436 | 406 | 27.2 |
| NS4 | 26–27 Jan 2012 | 2005 | AL, GA, SC | Slight<br>Tornado | 418 | 98 | 26.3 |
| NS5 | 23–24 Feb 2012 | 0040 | AL, GA, TN | Slight | 584 | 611 | 32.4 |
| NS6 | 16 Dec 2012 | 1520 | AL, MS | Slight | 506 | 228 | 25.3 |
| S1 | 29 Jan 2008 | 1650 | IL, IN, KY, TN | Moderate<br>Tornado, severe thunderstorm | 72 | 213 | 31.7 |
| S2 | 5–6 Feb 2008 | 2310 | KY, TN | High<br>Tornado, severe thunderstorm | 927 | 632 | 35.5 |
| S3 | 26 Feb 2008 | 1040 | AL, GA | Slight<br>Tornado, severe thunderstorm | 813 | 861 | 33.7 |
| S4 | 18 Feb 2009 | 1910 | AL, GA | Moderate<br>Tornado, severe thunderstorm | 771 | 461 | 33.5 |
| S5 | 28 Mar 2010 | 1850 | NC, SC, VA | Slight<br>Tornado | 253 | 643 | 32.2 |
| S6 | 29–30 Nov 2010 | 0000 | AL, MS | Slight<br>Tornado | 315 | 741 | 36.6 |
| S7 | 24–25 Feb 2011 | 2250 | AR, IN, KY, MS, MO, TN | Moderate<br>Tornado, severe thunderstorm | 333 | 342 | 43.6 |
| S8 | 28 Feb 2011 | 1515 | GA, KY, NC, SC, TN, VA | Moderate<br>Tornado, severe thunderstorm | 533 | 822 | 36.9 |
| S9 | 29–30 Jan 2013 | 0105 | AL, AR, IL, IN, KY, MO, TN, MS | Moderate<br>Tornado, severe thunderstorm | 248 | 455 | 34.1 |
| S10 | 10 Feb 2013 | 1720 | AL, MS | Slight<br>Tornado | 281 | 753 | 32.2 |
| S11 | 21–22 Dec 2013 | 2030 | AR, IN, KY, MS, OH, TN | Moderate<br>Tornado, severe thunderstorm | 286 | 548 | 35.3 |

Recent research has corroborated these findings, suggesting that cool season HSLC events in the Mississippi, Tennessee, and Ohio valleys, as well as the Southeast and mid-Atlantic regions, may rely more heavily on the synoptic environment than severe thunderstorms and tornadoes during the warm season in the plains (e.g., Gaffin and Parker 2006; Trier et al. 2006; Coniglio et al. 2007; Thompson et al. 2008; Wheatley and Trapp 2008; Tochimoto and Niino 2016). Synoptic forcing is commonly stronger during the cool season, enabling convection to be initiated in lower-CAPE environments (Schumacher and Johnson 2005; Brooks 2009). Synoptic systems, particularly midlatitude cyclones with associated warm and cold fronts, enable and enhance convection in low-CAPE environments by providing strong, large-scale

convergence and lift (e.g., Jewett and Wilhelmson 2006; Lane and Moore 2006; Brooks 2009; Clark 2009; Dial et al. 2010; Clark 2013). Advection of warm, moist air in the warm sector of a midlatitude cyclone in addition to heat fluxes within the boundary layer may also contribute to increases in CAPE ahead of an approaching cold front (e.g., Brooks 2009; Tochimoto and Niino 2016).

In some low-CAPE environments, instability may also increase through the release of potential instability (Clark 2009; Lane and Moore 2006; Evans 2010; Sherburn and Parker 2014). In many warm season, nonsynoptically forced environments, potential instability release can be driven by cold pool lifting; however, in cool season, low-CAPE environments, synoptic ascent appears to be the primary driver of potential instability release (e.g., Clark 2009; Evans 2010). Ongoing research (e.g., Sherburn et al. 2016) has shown that southeastern U.S. severe thunderstorm environments with 0–3-km shear $\geq 18\,\mathrm{m\,s^{-1}}$ and CAPE $\leq 500\,\mathrm{J\,kg^{-1}}$ typically occur in the warm sector of a midlatitude cyclone and that potential instability combined with vertical motion ahead of an upper trough and cold front commonly attend severe convection.

Taken altogether, the literature reveals that low-CAPE severe thunderstorms are a common and important forecasting challenge, especially in the southern and eastern United States. Idealized modeling studies have revealed some of the fundamental processes in HSLC environments, but it is clear that HSLC events are often accompanied by strong synoptic forcing as well as large-scale support for destabilization (e.g., McCaul and Weisman 2001; Jewett and Wilhelmson 2006; Wheatley and Trapp 2008; Brooks 2009; Kirkpatrick et al. 2011). The goal of this particular research is to determine the environmental conditions necessary for HSLC severe convection to occur and the mechanisms by which these conditions are met. The following section details the experimental design of a modeling study that aims to improve our understanding of these large-scale processes.

## 2. Methods

As reviewed above, it appears that synoptic and mesoscale forcing may produce rapid destabilization of low-CAPE environments, especially during the cool season. Modifications to the low-level environment that enhance severe convection may occur on relatively short temporal scales, possibly on the order of an hour or less. Storm-scale observational data are not typically readily available for these types of events in the southeastern United States, and many operational model analyses do not have the appropriate temporal resolution (i.e., subhourly) necessary for depicting the processes by which the environment may change over a short amount of time. Thus, case study model simulations utilizing real initial conditions are used for this research.

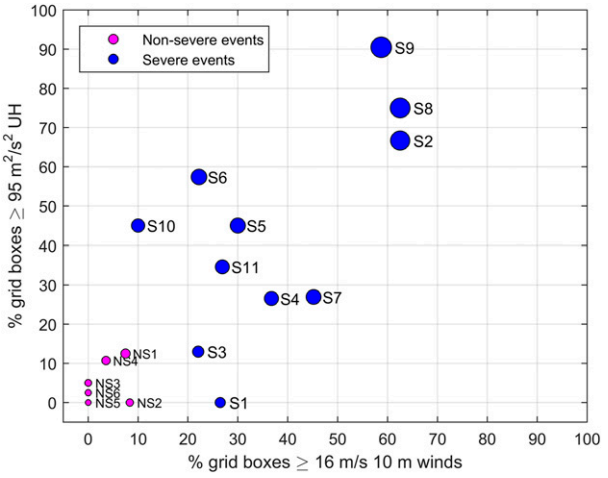


FIG. 1. Percentage of $50 \times 50$ grid-point boxes containing at least one grid point reaching a 10-m wind speed of $16\,\mathrm{m\,s^{-1}}$ at some point during the defined time period ($x$ axis). Percentage of $50 \times 50$ grid-point boxes containing at least one grid point reaching a 1–3-km UH value of $95\,\mathrm{m^2\,s^{-2}}$ within the defined time period ($y$ axis). The sizes of the dots in the plot are analogous to the sum of the percentage of boxes meeting the threshold for UH and percentage of boxes meeting the threshold for 10-m winds. Points are numbered chronologically within subsets of nonsevere events and severe events, as in Table 1.

### a. Experimental design

Numerical simulations of severe and nonsevere events, defined in the following section, were performed using the fully compressible, nonhydrostatic Advanced Research version of the Weather Research and Forecasting (WRF-ARW; Skamarock et al. 2008) Model, version 3.5.1. To capture both synoptic and mesoscale processes, an outer domain with 9-km horizontal grid spacing was one-way nested down to a convection-allowing 3-km grid. The positions of the grids differed for each simulation depending on the particular region of interest for each case. Vertical grids in both domains contained 50 levels with a model top pressure at 50 hPa and vertical stretching (including 11 levels in the lowest kilometer).

Initial and lateral boundary conditions for each simulation were supplied by the North American Mesoscale (NAM) model 12-km analyses. Lateral

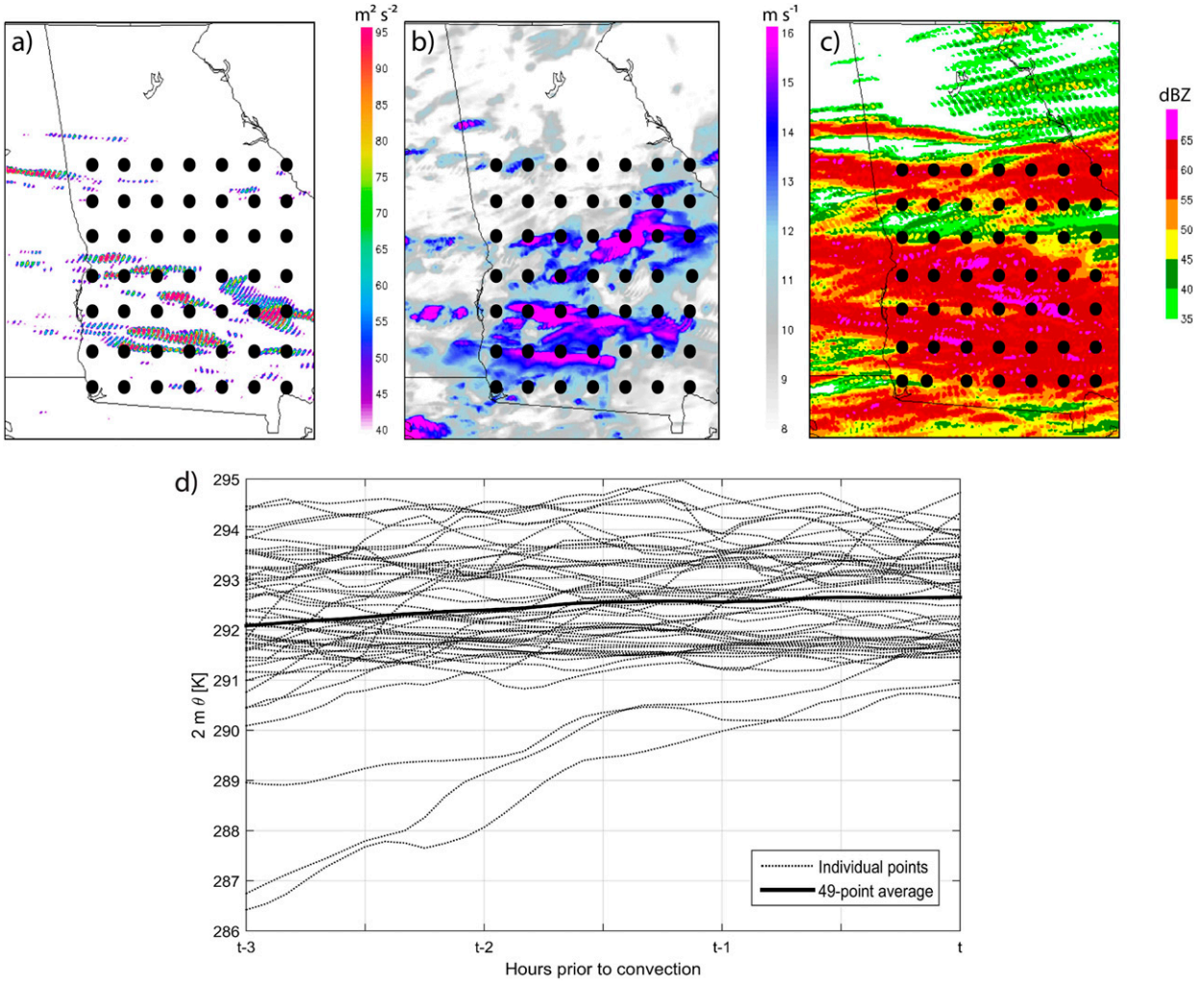


FIG. 2. The area that was broken up into 50 × 50 grid-point boxes for the case simulation of 18 Feb 2009 (S4). Maxima of (a) 1–3 km UH ($m^2 s^{-2}$), (b) 10-m winds ($m s^{-1}$), and (c) composite reflectivity (dBZ). (d) The 3-h time series of 2-m potential temperature (K) for each of the 49 points (dotted lines) for the case simulation of 18 Feb 2009 (S4). The 3-h average of all 49 points is also shown (thick solid line). This type of average will be shown and referred to throughout the manuscript.

boundaries were updated every 6 h. Convection on the 9-km domain was parameterized by the Kain–Fritsch scheme (Kain 2004); convection was simulated explicitly on the 3-km domain. Land surface interactions were represented by the Noah land surface model (Chen and Dudhia 2001). Boundary layer and microphysical processes were parameterized by the nonlocal Yonsei University scheme (YSU; Noh et al. 2003) and the WSM6 graupel scheme (Hong and Lim 2006), respectively. The Rapid Radiative Transfer Model (RRTM) longwave radiation scheme (Mlawer et al. 1997) and the fifth-generation Pennsylvania State University–National Center for Atmospheric Research Mesoscale Model (PSU–NCAR MM5), known operationally as the Dudhia shortwave radiation scheme (Dudhia 1996), were also used in the model. Simulations were run for a minimum of 30 h in order to account for the evolution of the synoptic and mesoscale environments during the day leading up to, as well as during, the event.

Philosophically, the purpose of the simulations was not to replicate the exact events that occurred, but to study modeled processes of a population of severe events and nonsevere events. Keeping the model configuration the same for each simulation allowed for comparison of processes among the simulations without differences attributed to changes in physical parameterizations. Although exact replication of a particular event was not a goal, simulated reflectivity was subjectively compared to the observed reflectivity to ensure

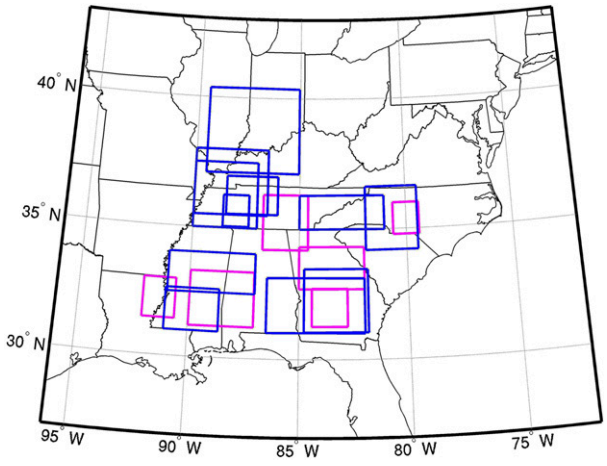


FIG. 3. Outlines of all seventeen 7 × 7 grid-point boxes for which average time series were calculated. Severe events are outlined in blue, and nonsevere events are outlined in magenta.

that each simulation produced a reasonably realistic result (not shown). Sea level pressure and surface-based CAPE (SBCAPE) were compared to observations (not shown) and archived Storm Prediction Center (SPC) mesoanalysis data (Table 1), referred to as surface objective analyses (SFCOA; Bothwell et al. 2002), to provide additional assurance of reasonably simulated environmental ingredients.

### b. *Case study selection*

Selection of severe events and nonsevere events was guided by collaboration with National Weather Service operational meteorologists across the Ohio and Mississippi valleys and the southeastern United States. Criteria for identifying HSLC events have varied among previous researchers. Recent studies used an upper limit of 500 J kg$^{-1}$ of analyzed mixed layer CAPE (MLCAPE) or SBCAPE along with 0–6-km bulk shear of 18 m s$^{-1}$ or greater (Guyer and Dean 2010; Davis and Parker 2014; Sherburn and Parker 2014). In examining previously studied HSLC events, it was discovered that in some cases, observed SBCAPE values may have increased past 500 J kg$^{-1}$ just before severe convection occurred. In addition, many cool season severe events occur in environments with SBCAPE values between 500 and 1000 J kg$^{-1}$, especially along the Gulf Coast (e.g., Smith et al. 2008). Thus, for this study, a threshold of 1000 J kg$^{-1}$ of SBCAPE was used. It is not a practical expectation for the thermodynamic characteristics of the simulated environments to be identical to the SFCOA; however, each simulation was compared to the SFCOA gridded dataset to ensure that maximum SBCAPE throughout the entire simulated time over the corresponding area

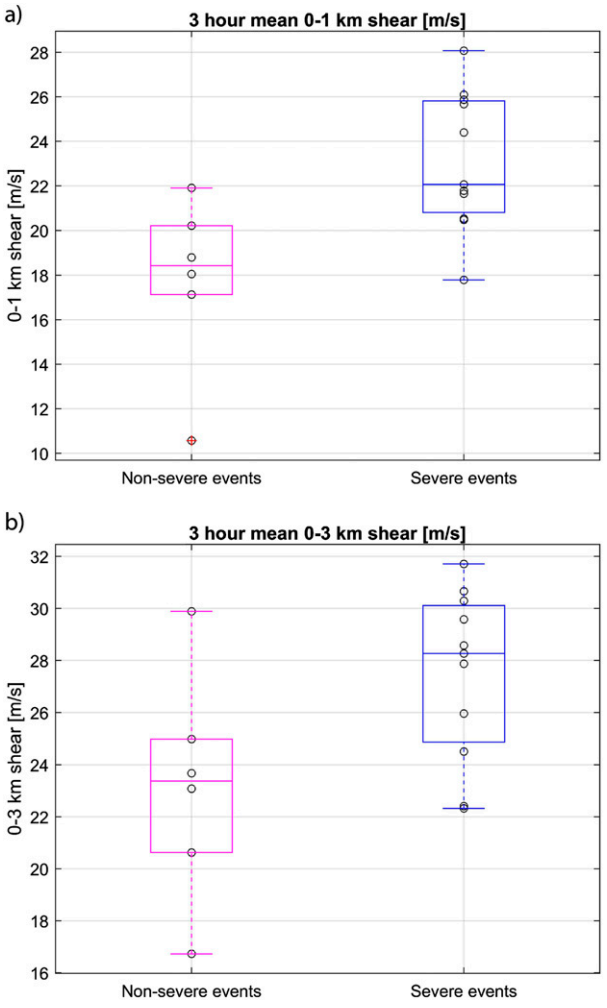


FIG. 4. Box-and-whisker plots for the 3-h mean (a) 0–1-km shear (m s$^{-1}$) and (b) 0–3-km shear (m s$^{-1}$), averaged over 49 points for each case as discussed in section 2d. The magenta and blue plots show the values for nonsevere events and severe events, respectively. The black circles indicate the values of the 3-h mean shear for each individual event.

was ≤1000 J kg$^{-1}$ in both the simulations and the SFCOA (Table 1). All cases selected also had maximum simulated 0–3-km shear values[2] much greater than 18 m s$^{-1}$ over a large portion of the domain (Table 1).

Each of the severe events included multiple SPC reports of tornadoes, multiple severe and/or significant severe winds, and, in some cases, hail. A case was defined as a nonsevere event if a slight risk or greater SPC

[2] Recent work has determined that the lower-tropospheric (i.e., within the lowest 3 km) wind shear is an adequate predictor of the severity of an HSLC convective environment (e.g., Schneider et al. 2006; Sherburn and Parker 2014).

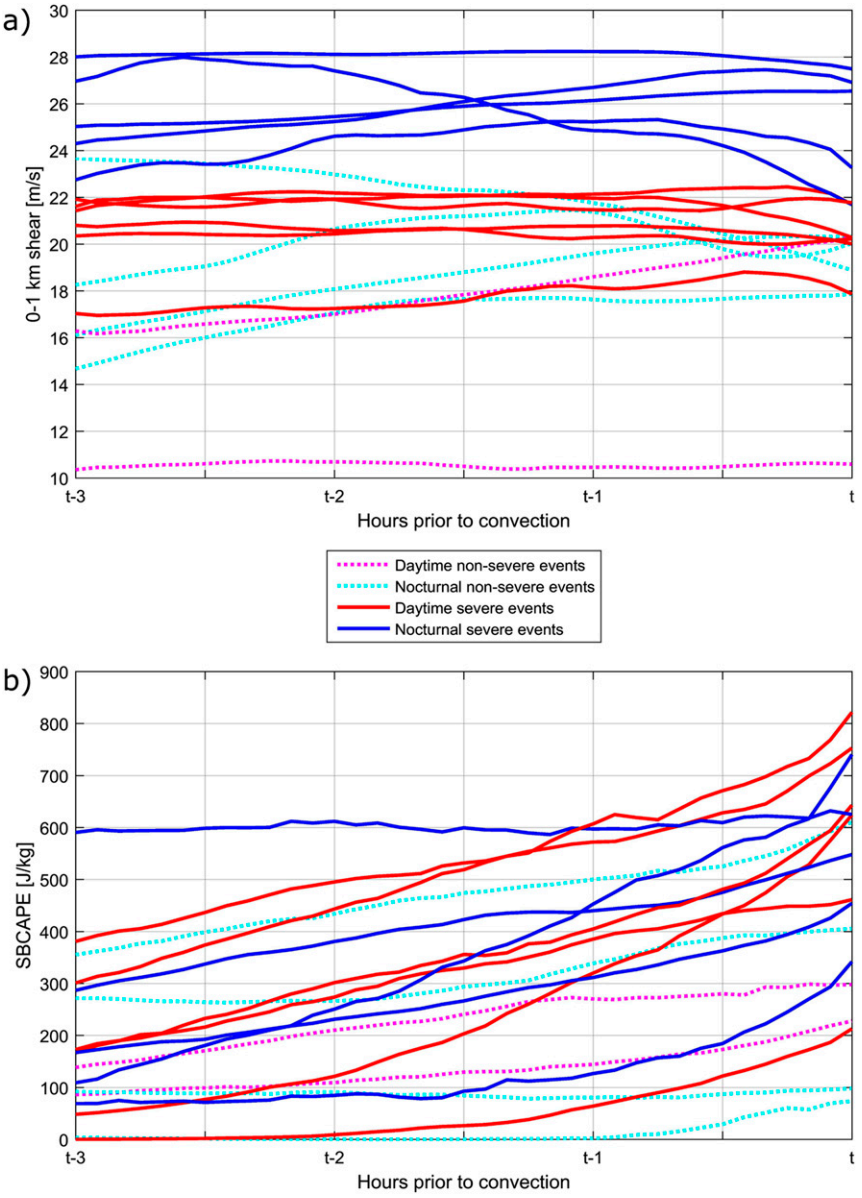


FIG. 5. Average time series of (a) 0–1-km shear ($m\,s^{-1}$) and (b) SBCAPE, calculated and averaged over 3 h for all 49 points for each case as described in section 2d. Red and magenta lines represent cases with an ending time before 1930 LT, whereas blue and cyan lines represent cases with an ending time after 1930 LT. Time series for severe events are plotted as solid lines; time series for nonsevere events are plotted as dotted lines.

outlook and/or an SPC severe thunderstorm or tornado watch was issued for a particular area and no severe local storm reports occurred within a broad region of the outlook and/or watch (in other words, false alarm events; see Table 1). Eleven severe events and six nonsevere events fitting these criteria were simulated using the model configuration described in section 2a. All cases selected occurred between 29 November and 30 March (i.e., the cool season) from 2007 through 2013 at varying hours throughout the day. The severe events and nonsevere events were intentionally selected from a broad region including the Gulf Coast, the area from the Mississippi valley through the Ohio valley, and the Southeast in order to determine general (location independent) similarities in HSLC events during the cool season. As previously mentioned, these regions have been identified as the most conducive to severe cool season HSLC convection.

### c. *Verification of simulated severe versus nonsevere events*

A basic quality check for our experimental design is to verify that simulated severe events actually produce stronger storms than simulated nonsevere events. For each simulated event, 1–3-km updraft helicity[3] (UH) was calculated instantaneously every 5 min on the 3-km domain following the method of Kain et al. (2008). Peak 10-m winds were also calculated. The area size and location for these calculations was expanded or contracted to closely frame the HSLC SPC reports for the severe events and the HSLC SPC outlook/watch area for nonsevere events. The area was divided into 50 × 50 grid-point boxes (i.e., 150 km × 150 km boxes). For each case, the number of 150 km × 150 km boxes containing at least one grid point within the range of different threshold values of UH and peak 10-m winds was summed and normalized by the total area.[4] From experimentation with various thresholds, 95 $m^2 s^{-2}$ UH and 16 $m s^{-1}$ 10-m wind values clearly separate the strongest simulated storms from grid-scale noise and large-scale environmental flow. The simulated nonsevere events were clearly weaker than the simulated severe events based on these defined thresholds of 1–3-km UH and 10-m winds, given the placement of the 50 × 50 grid-point boxes for each case (Fig. 1). Again, exact correspondence to observed cases was not expected, but these metrics provide confidence that modeled severe events were appreciably different from modeled nonsevere events.

### d. *Time series calculations*

To determine the mechanisms by which the simulated environments changed over time, a region of the most intense HSLC convection was identified subjectively based upon reflectivity, UH, and 10-m winds. Environmental evolution in these regions was studied by constructing time series of multiple environmental variables leading up to the most intense convection. A rectangle of 49 points (7 $x$ points × 7 $y$ points) was positioned within the HSLC region with the most intense 1–3-km UH and 10-m winds in addition to the highest reflectivity over the period of time defined in the previous section (an example is shown in Fig. 2). For each of the 49 points, an "event relative" 3-h time series was constructed. The ending time at each individual grid point was defined as the time of maximum SBCAPE within the 20 min prior to passage of reflectivity ≥ 35 dBZ. Each of the 49 points could have a different ending time, and each point's event-relative 3-h time series was then averaged to provide prevailing trends in the preconvective environment. An example of an averaged time series is shown in Fig. 2d (thick bold line), as constructed from the 49 individual points (thin dotted lines). The following sections will refer to this average 3-h time series for each case.

Outlines of the 7 × 7 point rectangles for all cases are shown in Fig. 3. Within a single event, all $x$ points were identically spaced and all $y$ points were identically spaced, though the spacing varied from case to case (Figs. 2 and 3). Evenly spacing the points ensured that calculations were performed over a general area of intense simulated convection rather than over a few handpicked points, preventing biased results. Varying the distances between the $x$ points and $y$ points for each case within the 49-point rectangles over time did not alter the results significantly. In cases with a large rectangle, experimentation showed that shrinking the area to one-half or one-third of the original size resulted in the fields becoming a bit less smooth; however, the overall trends and changes over time were not altered

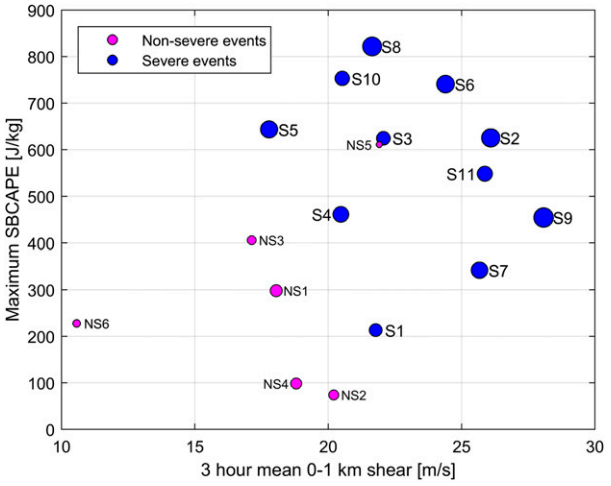


FIG. 6. The 3-h mean 0–1-km shear ($m s^{-1}$; $x$ axis) vs 3-h maximum SBCAPE ($J kg^{-1}$; $y$ axis) for all severe (blue) and nonsevere (magenta) events. Averages are calculated over 49 points for each case, as explained in section 2d. Sizes are based on UH and 10-m winds, as described in section 2c, and are shown in Fig. 1. Points are numbered chronologically within subsets of nonsevere events and severe events, as in Table 1.

[3] The 1–3-km UH was used as opposed to the conventional 2–5-km UH because of the shallow nature of the rotation and updrafts in HSLC events (McCaul and Weisman 1996; Smith et al. 2012; Davis and Parker 2014; Sherburn and Parker 2014).

[4] The purpose of calculating the percentage of 150 km × 150 km boxes with maximum values meeting the thresholds for UH and 10-m winds as opposed to the percentage of total grid points was to identify more widespread severe simulated convection within a particular event (i.e., this method prevents small clumps of intense UH or 10-m winds).

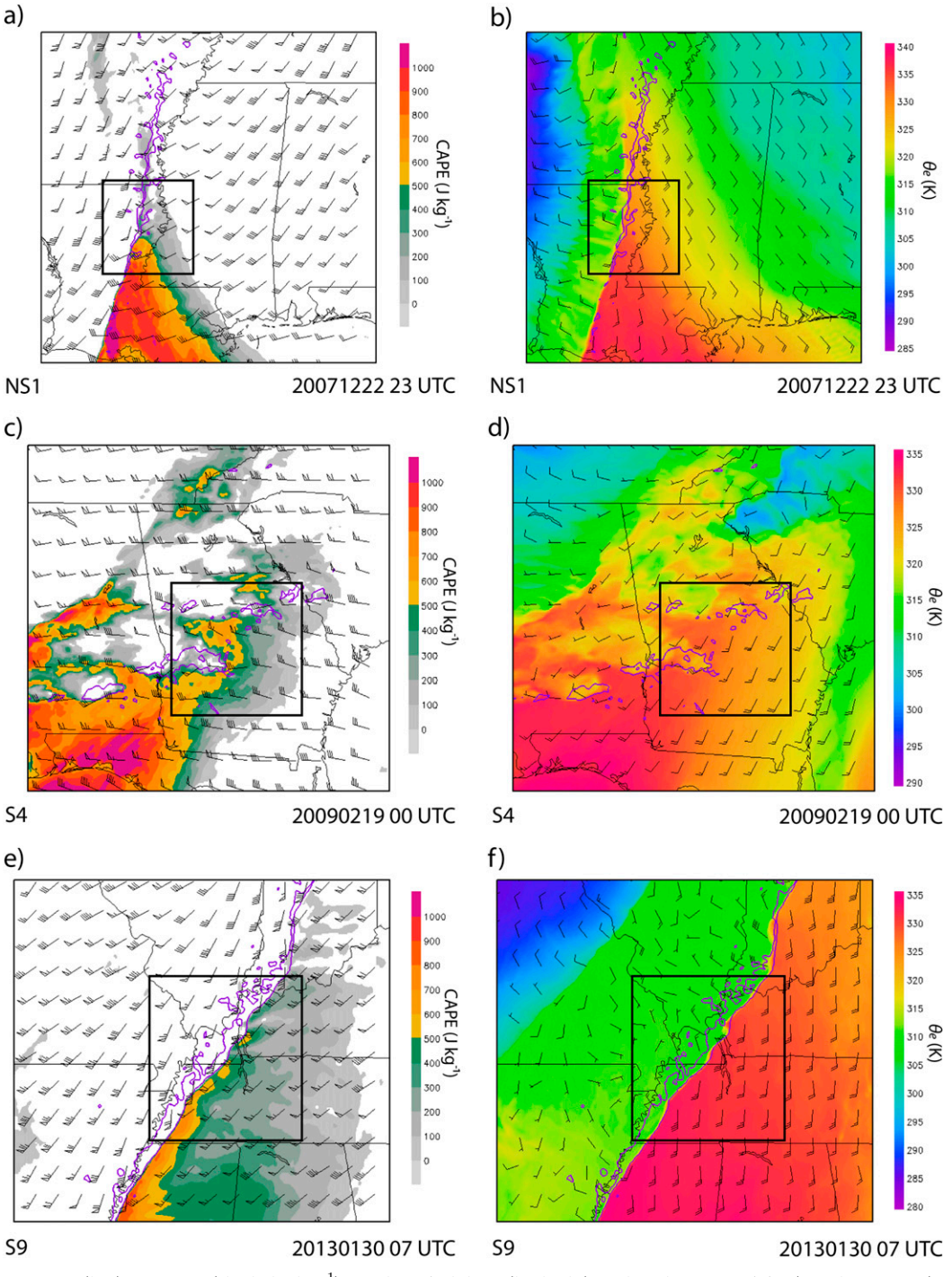


FIG. 7. (left) SBCAPE (shaded; J kg$^{-1}$), 0–3-km wind shear (barbs; kt), and 40-dB$Z$ reflectivity (purple contours). (right) The 10-m equivalent potential temperature (shaded; K), 10-m wind (barbs; kt), and the 40-dB$Z$ reflectivity (purple contours) for (a),(b) 23 UTC 22 Dec 2007 (NS1), (c),(d) 0000 UTC 19 Feb 2009 (S4), and (e),(f) 0700 UTC 30 Jan 2013 (S9). The black box indicates the 7 × 7 grid-point box used for calculations (i.e., the area of interest). Plots are taken from the 3-km simulated grid.

(not shown). Using 49 points for time series averaging regardless of box size was intended to ensure that an equal number of time series contributing to the average was used among all cases. This particular size selection was chosen so as to keep the points at a reasonable distance from one another for the simulated case with the smallest area of convection, while still having a large enough number to make a smooth average.

## 3. Results and discussion

### a. Overview of simulated environments

All 17 of the present cases had strong observed 0–3-km shear, as was required to qualify them as "high shear" events (refer to Table 1). All but one simulated case had 3-h mean[5] 0–1-km shear greater than 17 m s$^{-1}$ (Fig. 4a). Consistent with the findings of Sherburn and Parker (2014), the highest 3-h mean 0–1-km shear in a nonsevere event was less than the median 3-h mean 0–1-km shear for the severe events (Fig. 4a). The 3-h mean 0–3-km shear magnitudes for all cases were greater than 16 m s$^{-1}$, with the 3-h mean for some cases reaching close to or above 30 m s$^{-1}$ (Fig. 4b). However, in this sample, the 3-h mean 0–3-km shear values did not distinguish the severe events from the nonsevere events as well as the average values of mean 0–1-km shear.

Previous research has identified that nocturnal events are typically influenced by enhanced low-level shear as a result of the presence of a nocturnal low-level jet (LLJ; e.g., Kis and Straka 2010). The 0–1-km shear did more clearly distinguish the severe events from the nonsevere events when examining nocturnal[6] cases and daytime cases separately. All simulated nocturnal severe events had higher 0–1-km shear than all simulated nocturnal nonsevere events in the hours leading up to convection (cyan and blue curves in Fig. 5a). These large nocturnal shear values may be partly linked to the development of the nocturnal LLJ, although it should be noted that any trends in 0–1-km shear are quite weak in the 3 h prior to convection (Fig. 5a). Because of the small number of nonsevere daytime events, it is difficult to identify whether the same separation exists in the daytime cases, though most of the daytime severe events do have higher 0–1-km shear than the two daytime nonsevere events (Fig. 5a). The uniformity of the 0–1-km shear throughout

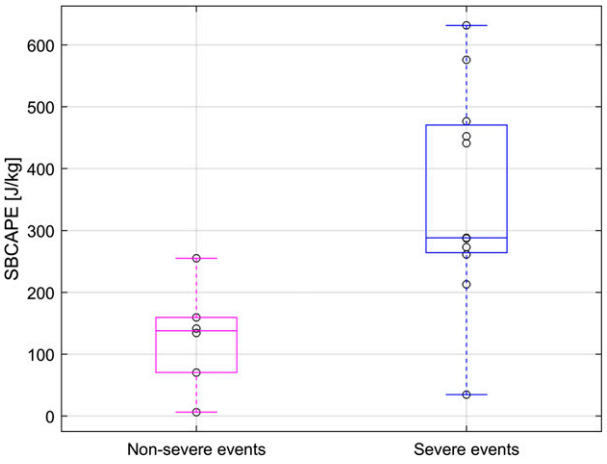


FIG. 8. As in Fig. 4, but for the 3-h change in SBCAPE.

the time series suggests forecasters may be able to treat the low-level vertical shear as "steady" when making short-term forecasts. However, CAPE rapidly increases over time (Fig. 5b), in some cases from less than 60 J kg$^{-1}$ to greater than 600 J kg$^{-1}$ in less than 3 h. It is clear that by the time of arrival of convection, *most nonsevere events had lower maximum SBCAPE and 0–1-km shear values than did severe events* (Fig. 6). Unlike the comparatively steady shear component, the CAPE differences may emerge on time scales $\leq$ 3 h (Fig. 5b). Thus, the next sections will focus primarily on the thermodynamic evolution of the simulated environments.

### b. Destabilization of the preconvective environment

Although the characteristics of the environment and the modes of convection varied among the cases, all simulated severe events and nonsevere events occurred within a warm sector and a relatively narrow swath of comparatively high equivalent potential temperature $\theta_e$ (Figs. 7b,d,f), generally in association with a midlatitude cyclone. Some events occurred as an organized quasi-linear convective system (QLCS) along a linear boundary (i.e., a cold front or a linear outflow boundary; Figs. 7a,b,e,f), while other events occurred as more isolated convection within the warm sector of a midlatitude cyclone (Figs. 7c,d). In short, simulated HSLC convection tended to occur within a region of strong, southerly, or southwesterly flow and very warm, moist air in advance of an outflow or synoptic-type boundary.

Interestingly, averages (calculated as described in section 2d) of SBCAPE in all simulated severe environments except for one (event S2), and all nonsevere environments, were less than 400 J kg$^{-1}$ just 3 h prior to convection (Fig. 5b). Every case exhibited some amount of destabilization (i.e., increase in CAPE) over the three

[5] The term 3-h mean refers to the average value of the 49 point-averaged 3-h time series for each case.

[6] Throughout the manuscript, events occurring from 1930 to 0700 local time (LT) will be referred to as nocturnal events. Events occurring from 0700 to 1930 LT will be referred to as daytime events.

TABLE 2. Changes in SBCAPE (J kg$^{-1}$) over 3 h for all simulated severe events and nonsevere events, averaged over all 49 points as described in section 2d. The first column identifies the event. The second column displays the CAPE change attributed to the lowest model-level mixing ratio change (green bars in Fig. 9). The third column displays the CAPE change attributed to the change in lowest model-level temperature (red bars in Fig. 9). The fourth column corresponds to the blue bars in Fig. 9, displaying the CAPE change attributed to the temperature change at all levels minus the CAPE attributed to the temperature change at the lowest model level. The sum of columns 2–4 is shown in column 5, and the total grid-calculated CAPE change (black bars in Fig. 9) is shown in the last column. All values of CAPE change are in J kg$^{-1}$.

| Case ID | CAPE change due to surface $q_v$ | CAPE change due to surface $\theta$ | CAPE change due to $\theta$ aloft | Sum of CAPE changes by three mechanisms | Actual CAPE change |
|---|---|---|---|---|---|
| NS1 | 267.3 | 16.0 | −90.7 | 192.6 | 159.4 |
| NS2 | 31.0 | −2.4 | 16.9 | 45.5 | 70.4 |
| NS3 | 378.8 | −128.9 | 19.1 | 269.0 | 134.3 |
| NS4 | 11.6 | −0.3 | 48.6 | 59.9 | 6.2 |
| NS5 | 247.7 | −67.6 | 114.9 | 295.0 | 255.1 |
| NS6 | 43.7 | −1.9 | 89.8 | 131.6 | 141.4 |
| S1 | 6.0 | 13.8 | 82.7 | 102.5 | 212.8 |
| S2 | 134.4 | 102.3 | −143.0 | 93.7 | 34.6 |
| S3 | 173.0 | 259.0 | 5.9 | 437.9 | 575.9 |
| S4 | 241.3 | 20.1 | 12.4 | 273.9 | 288.3 |
| S5 | 307.6 | 137.9 | −3.8 | 441.7 | 476.5 |
| S6 | 297.4 | 110.9 | 21.0 | 429.3 | 631.5 |
| S7 | 46.3 | 6.9 | 115.8 | 169.1 | 273.0 |
| S8 | 201.4 | 62.0 | 195.3 | 458.7 | 440.8 |
| S9 | 84.5 | 60.5 | 113.8 | 258.8 | 287.3 |
| S10 | 341.6 | 153.2 | −51.2 | 443.6 | 452.0 |
| S11 | 159.2 | 70.4 | 55.7 | 285.3 | 261.3 |

final hours prior to convection, including the nocturnal cases for which diurnal heating was absent (Fig. 5b). Some severe environments experienced SBCAPE increases of over 600 J kg$^{-1}$ over 3 h; this has significant implications for forecasting, as model output is often viewed at 3- or 6-hourly intervals. The nonsevere events tended to have a smaller increase in SBCAPE over time than the severe events (Figs. 5 and 8). In fact, the maximum increase in SBCAPE over 3 h in a nonsevere environment was lower than the 25th percentile increase in the severe environments. It should be noted that MLCAPE was also calculated to ensure that MLCAPE and SBCAPE were not substantially different. All MLCAPE values were similar to those of SBCAPE (correlation of 0.9761); thus, SBCAPE is used for calculations throughout the remainder of the manuscript.

The primary means of generating or amplifying SBCAPE include increasing temperatures near the surface, increasing moisture near the surface, and decreasing temperatures aloft. To determine the contribution of each of these components to the overall destabilization of the environment, time series of SBCAPE were calculated by isolating the unique contributions of the surface[7] mixing ratio $q_v$, the surface potential temperature $\theta$, and $\theta$ aloft. For example, to assess the contribution of the change in potential temperature near the surface to the overall destabilization, a 3-h time series of SBCAPE was calculated while holding the entire profile of temperature and moisture constant (i.e., at the initial values of the time series) and only updating surface $\theta$ with time. Similar calculations were performed by updating only surface $q_v$ with time. To determine the contribution of cooling aloft, the calculations were performed updating $\theta$ at all levels with time, then subtracting the contribution obtained by updating only the surface $\theta$. Separating the effect of changing the surface temperature from the effect of changing temperatures aloft isolates the two contributions to the lapse rate, yielding more information about which mechanisms are most important in the conditioning of HSLC environments. The three calculated contributors did not exactly sum to the total change in SBCAPE,[8] but they are generally quite close (refer to Table 2) and help illustrate which processes were most important in the destabilization of the simulated HSLC environments.

Although it is not possible to show a detailed case study for every one of the 17 simulated cases, it is useful

[7] The surface calculations refer to the lowest model level.

[8] This is largely because $\theta_e$ is not a perfectly linear function of $\theta$ and $q_v$, and because we have neglected any changes in $q_v$ aloft, which also alter the environmental virtual potential temperature $\theta_v$ profile (and thus the calculated CAPE).

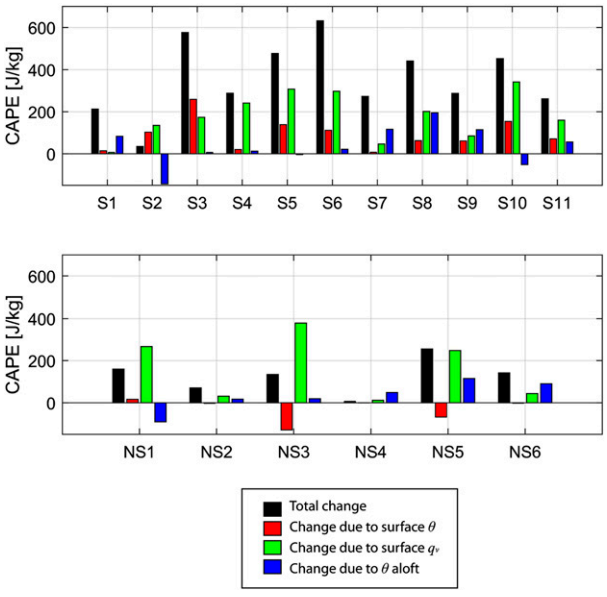


FIG. 9. Changes in SBCAPE ($J\,kg^{-1}$) over 3 h for all simulated severe events and nonsevere events, averaged over all 49 points as described in section 2d. All black bars show the change in total grid-calculated CAPE. Red bars show the CAPE change attributed to change in lowest model-level temperature. Green bars show the CAPE change attributed to the lowest model-level mixing ratio change. Blue bars show the CAPE change attributed to the temperature change at all levels minus the CAPE attributed to the temperature change at the lowest model level. Cases are ordered chronologically among the severe and nonsevere events as in Table 1.

to study their net CAPE changes in bulk. As mentioned in section 3a, the total increase in SBCAPE was generally larger during severe events than nonsevere events (black bars in Fig. 9). One severe event (S2) did have relatively small increases in SBCAPE; however, this severe event was unusual in that it occurred along a near-stationary warm front (not shown), which allowed relatively moderate CAPE values ($\sim 600\,J\,kg^{-1}$) to persist throughout the time series (top blue line in Fig. 5b). Surface moistening contributed to a portion of the increases in SBCAPE for all severe events and nonsevere events (green bars in Fig. 9, Table 2), which is unsurprising given the ample flow from the Gulf of Mexico that was present during all events (e.g., Fig. 7). Two nonsevere events (NS1, NS3) and one severe event (S2) had predominant contributions from surface moistening that were offset by surface cooling (NS3; Fig. 9) or warming aloft (S2, NS1; Fig. 9). Thus, although moistening near the surface is a unifying ingredient in destabilizing the environment of all cases, the case-to-case variations in temperature trends may be more important in constraining the overall CAPE changes.

Severe events tended to occur in environments destabilized by surface warming, while surface cooling may have been detrimental to some nonsevere events. Two nonsevere events (NS3, NS5) had substantial negative contributions to SBCAPE as a result of surface cooling (Fig. 9, Table 2), and three others had near-zero contributions from changes in surface temperature (NS2, NS4, NS6). In other words, the nonsevere events tended to have decreasing or steady temperatures near the surface in the hours leading up to convection, while the severe event environments experienced surface warming (Fig. 10). In fact, even the nocturnal severe environments exhibited increasing surface temperatures (solid blue lines in Fig. 10). Although this analysis comprises a rather small population of simulated cases, it appears that the behavior of the surface temperature may be useful in discriminating between severe and nonsevere HSLC environments, and may provide more insight than the lapse rate alone. Of course, destabilization may also be enhanced by cooling aloft and/or increases in surface moisture, though the latter also occurs in all simulated nonsevere events. It should be noted that increasing moisture and decreasing temperature near the surface, which occurred in most nonsevere events (Fig. 9), resulted in lowering of the lifted condensation level (LCL) over time, while the LCL for most severe events remained the same or slightly increased over time. However, the LCL heights were not substantially different between the severe events and the nonsevere events at the time of convection (not shown); all mean LCL heights were below 600 m above ground level, which would be considered quite low within the context of previous tornado climatologies (e.g., Thompson et al. 2003). A lower LCL is typically considered more favorable for severe convection, particularly tornadoes (e.g., Thompson et al. 2003). However, based on the above analysis, it may be that in limited CAPE environments, increasing temperatures near the surface provide a destabilization benefit that is more important than small changes in LCL heights.

In analyzing the temperature changes both at the surface and aloft, it appears that a combination of warming near the surface and cooling aloft (i.e., increasing the lapse rate) may be especially important in HSLC severe events. This seems to correspond with the apparent skill of low-level lapse rates in identifying severe HSLC environments (Sherburn and Parker 2014). The contribution from the cooling temperatures aloft varied from case to case, depending upon the availability of potential instability (PI) and forcing for ascent (as seen in the composite soundings for events S9 and S10 in Fig. 10), or other mechanisms by which cooling aloft may occur such as a cold front aloft (Hobbs et al. 1996; Rose et al. 2002), cold advection, ascending motion, or some combination of mechanisms. In some cases,

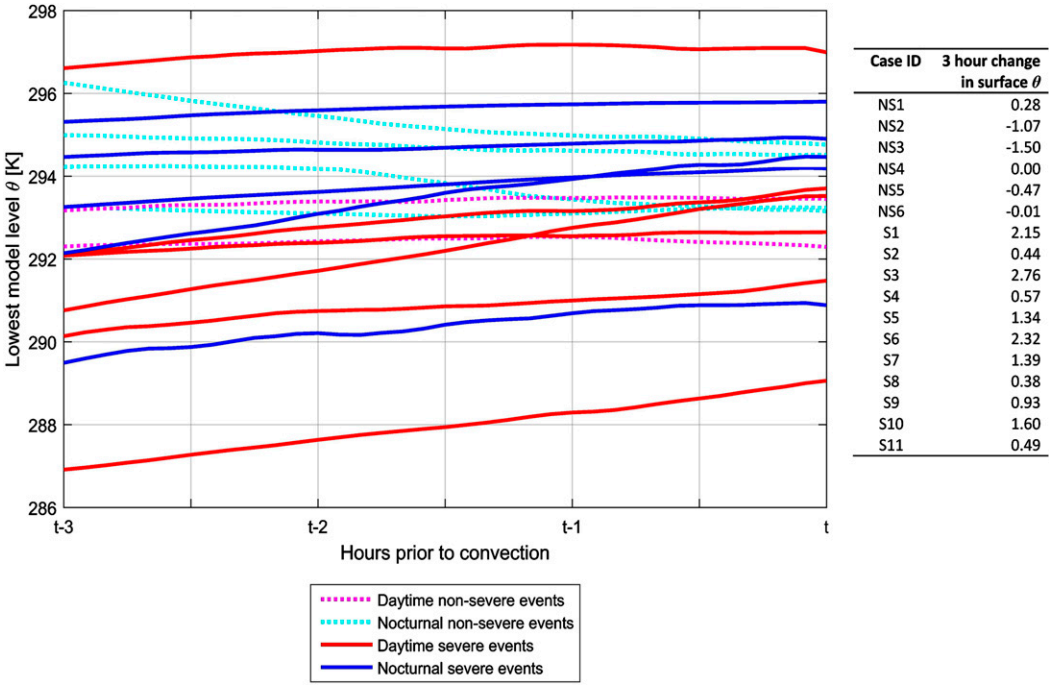


| Case ID | 3 hour change in surface $\theta$ |
|---|---|
| NS1 | 0.28 |
| NS2 | -1.07 |
| NS3 | -1.50 |
| NS4 | 0.00 |
| NS5 | -0.47 |
| NS6 | -0.01 |
| S1 | 2.15 |
| S2 | 0.44 |
| S3 | 2.76 |
| S4 | 0.57 |
| S5 | 1.34 |
| S6 | 2.32 |
| S7 | 1.39 |
| S8 | 0.38 |
| S9 | 0.93 |
| S10 | 1.60 |
| S11 | 0.49 |

FIG. 10. As in Fig. 5, but for lowest model-level potential temperature (K).

warming occurred throughout portions of the vertical profile, partially offsetting the contributions to CAPE from the increases in temperature and moisture near the surface (as seen in the composite sounding for event S10 in Fig. 11b). The severe events in which temperatures aloft caused decreases in SBCAPE typically also had relatively large positive contributions from warming near the surface (e.g., S2, S5, S10; Fig. 9). In other words, in these cases, much of the lower–midtropospheric column was warming simultaneously (as might be expected in a zone of deep warm advection). Nonsevere event NS1 was somewhat unique in that warming aloft reduced CAPE in the absence of appreciable surface warming (Fig. 9). Meanwhile, many severe events had positive contributions to CAPE as a result of temperature changes both near the surface *and* aloft (e.g., S9, S11; Figs. 9 and 11a), even if the positive contributions were relatively small (e.g., S1, S4, S7; Fig. 9).

### c. *Synoptic environmental characteristics*

All simulated cases occurred in synoptic environments characterized by mid- and upper-level troughs, associated surface cyclones, cold fronts, and low, mid-, and upper-level jets. Synoptic forcing can provide many of the necessary ingredients for severe convection (e.g., Gaffin and Parker 2006; Thompson et al. 2008; Brooks 2009), including warm air and moisture advection near the surface, cooling in mid- and upper levels, and vertical motion due to jet and frontal circulations. The release of potential instability by large-scale forcing for ascent may be an important mechanism for destabilization, as destabilization by cooling aloft was prominent in multiple simulated environments (Figs. 9 and 11a).

The synoptic environments in which cool season HSLC events typically occur can provide strong flow from the south, transporting warm air from the Gulf into cooler continental regions. Likewise, many simulated events exhibited a narrow swath of high-$\theta_e$ air and strong southerly winds near the surface just ahead of HSLC convection (cf. Fig. 7). Thus, temperature advection (i.e., the change in temperature due purely to the horizontal movement of air throughout the boundary layer) is likely a fundamental mechanism by which the temperatures near the surface increase in the preconvective environment. All but two simulated events (S8, NS3; Fig. 12) experienced positive average surface temperature advection over the 3 h prior to convection (Fig. 12). The air throughout the boundary layer may also be warmed or cooled by the surface sensible heat flux (here, the heat transferred throughout the boundary layer from the surface); however, values of the model output surface sensible heat flux over the boundary layer were on an order of magnitude less than that of temperature advection (Fig. 12). In addition, all simulated events except for two (S8, NS6; Fig. 12) had *negative* average surface sensible heat flux. This seems reasonable, as soil temperatures are characteristically low during the cool season. Southerly flow brings unseasonably warm air over the cool surface, yielding negative sensible heat flux

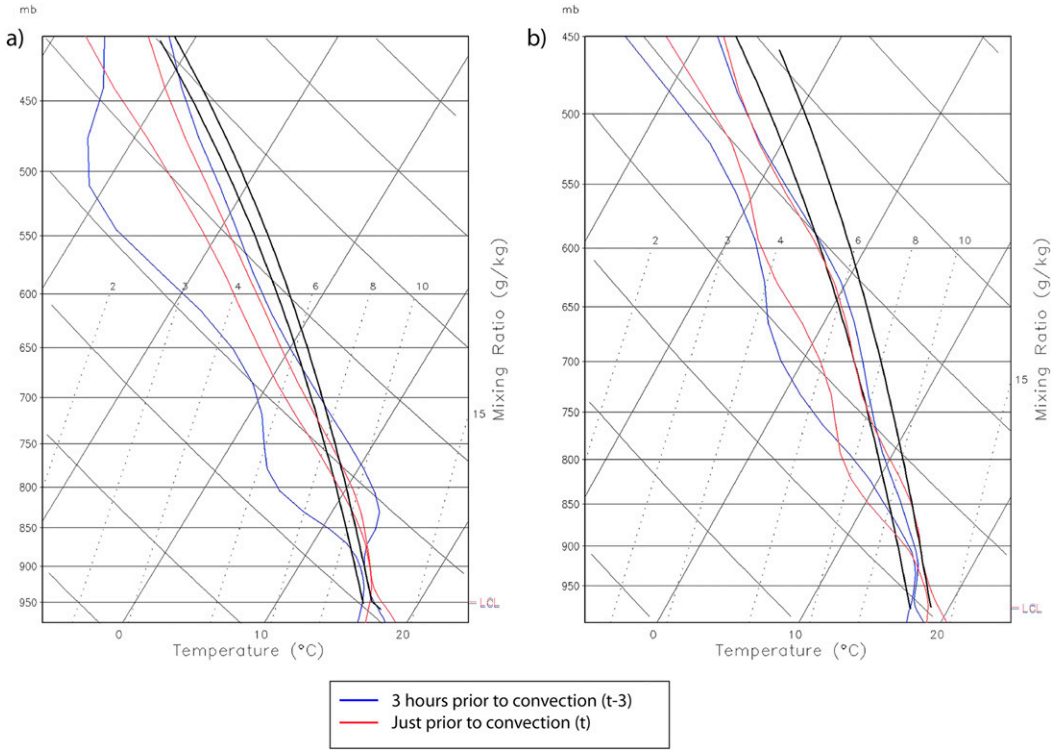


FIG. 11. Composite (of the 49 points used for the time series) skew $T$–log$p$ plots for (a) the 29–30 Jan 2013 simulated severe event (S9) and (b) the 10 Feb 2013 simulated severe event (S10). Blue lines indicate the composite sounding 3 h prior to the passage of convection, and red lines show a composite sounding just prior to convection (i.e., the final time in the time series). Boldface black lines indicate surface-based parcel paths. LCL heights are denoted at the bottom right of each panel.

(i.e., into the ground). In addition, all simulated preconvective environments existed in the warm sector of a midlatitude cyclone, yielding high cloud fractions (greater than 80% in all cases; not shown) that mitigated the ability for the ground to significantly warm by radiation during the day. Although other mechanisms for surface temperature change were not quantified (e.g., near-ground latent heat release), it does appear that warm advection near the surface was the primary mechanism responsible for surface warming. It should also be mentioned that just as the surface sensible heat fluxes are negative in all but two of the cases, the surface moisture fluxes are negative in all but one of the cases (not shown). In addition, the surface latent heat flux was most likely negative because of the advection of warm, moist air over cool, dry land that occurred in many of these cases. This indicates that the increases in CAPE due to $q_v$ (i.e., Fig. 9) are also largely attributable to horizontal advection. The combination of these two effects account for the very large northward transports of $\theta_e$ shown in Figs. 7b, 7d, and 7f.

Beyond these near-surface mechanisms, four severe events also exhibited apparent characteristics of destabilization by the release of potential instability (S3, S8, S9, S11). Although some other events appeared to exhibit minor destabilization through this mechanism, here we illuminate the process by focusing on the aforementioned four cases in which destabilization by the release of potential instability was most clear. The 3-h averages of 0–3-km $\theta_e$ lapse rates[9] and the 9-km grid-scale vertical motion[10] help depict this for each of the four severe events (Fig. 13). The decrease of $\theta_e$ with height in all four events indicates that a potentially unstable layer was present, and the median positive vertical

[9] The 0–3-km layer was used because most of the potential instability existed in this layer. In addition, ongoing research (e.g., Sherburn et al. 2016) has found this layer in combination with 3-km vertical velocity to be useful at indicating the conditions for the release of potential instability.

[10] The data for all calculations in this section were taken from the 9-km grid (due to grid noise in the vertical velocity field on the 3-km grid). The data were also spatially smoothed using the eight surrounding grid points in order to reduce the noise in the vertical velocity data. Data on the 9-km grid were only recorded every 30 min as opposed to every 5 min on the 3-km grid (as in previous sections); thus, it should be noted that the effects of the release of potential instability may be underrepresented. It is also possible that the 9-km grid removes potential instability too quickly because of its convective parameterization.

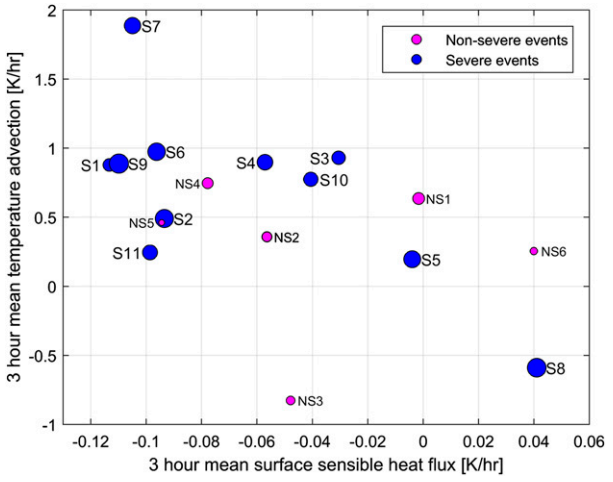


FIG. 12. As in Fig. 6, but for a 3-h average of sensible heat flux over the boundary layer ($K\,h^{-1}$; $x$ axis) vs a 3-h average of temperature advection over the boundary layer ($K\,h^{-1}$; $y$ axis).

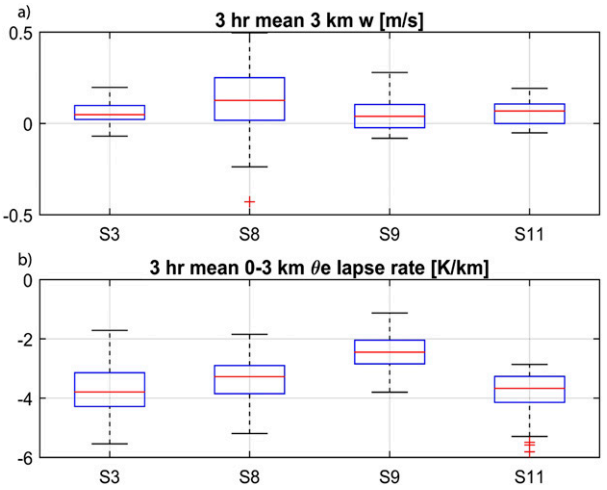


FIG. 13. (a) Box-and-whisker plots for the mean values of the (a) 3-km vertical velocity ($m\,s^{-1}$) and (b) 0–3-km equivalent potential temperature lapse rate ($K\,km^{-1}$) for each of the 49 points for each of S3, S8, S9, and S11 within the 3 h prior to convection. Data and calculations are from the 9-km grid, taken every 30 min, and spatially smoothed using the eight surrounding points for each of the 49 grid points.

motion demonstrates that lifting was present. Time series over 3 h (Fig. 14) show positive vertical velocities increasing as the frontal zone and associated convection approached. As vertical velocities increase, the $\theta_e$ lapse rates become less steep, the 3-km relative humidity increases, and cooling occurs at 3 km (Fig. 14). Lifting alone would be sufficient to cool and slightly destabilize a layer, but lifting of a potentially unstable layer to saturation would be most effective. Because the 49-point-averaged relative humidity trends toward 100% (and individual grid points and other levels do become saturated, e.g., Fig. 11a), it is likely that the potential instability present in the ambient environment was released across parts of the domain for each of the four simulated cases. An averaged trend toward 100% RH indicates that the release of potential instability is at least possibly occurring, providing a particularly effective means by which large-scale forcing for ascent may rapidly destabilize cool season, low-CAPE events in the 1–3 h prior to convection. It is certainly possible that the choice of PBL scheme may have some impact on the realization of potential instability in a simulated environment, as the temperature and moisture profiles are affected by the low-level mixing provided by the PBL scheme. The nonlocal YSU PBL scheme used for this research has been shown to represent the boundary layer in HSLC cases relatively well (e.g., Cohen et al. 2015); thus, other PBL schemes were not tested during this particular research.

## 4. Summary and future work

The goal of this study was to determine the synoptic and/or mesoscale processes that condition cool season HSLC environments and enable severe convection to occur. Clarifying the mechanisms by which the environment becomes a suitable host for HSLC convection is important in the short-term forecasting of HSLC events. To study multiple events on spatiotemporal scales not available through observations, simulations of 11 severe events and 6 nonsevere events occurring during November–March were performed using the WRF-ARW initialized and updated with NAM analysis data. A convection-allowing inner domain of 3 km enabled analysis of the synoptic-to-mesoscale processes occurring within the preconvective environment.

Destabilization of the preconvective environment was investigated for all simulated severe and nonsevere events. All cases were found to have some increase in SBCAPE in the 3 h prior to convection; however, severe events typically had much larger increases than nonsevere events. Some severe events had SBCAPE increases over $600\,J\,kg^{-1}$ in only 3 h, which are quite physically meaningful in environments that generally begin with SBCAPE $< 400\,J\,kg^{-1}$. Contributions of surface temperature, surface moisture, and temperatures aloft to SBCAPE were examined for each simulated case. The processes by which destabilization occurred in each of the 17 simulations varied considerably. Surface moistening contributed to an increase in CAPE for every simulation (Fig. 9). Surface warming increased CAPE in all 11 severe events, but only 1 nonsevere event (Fig. 9). Warm air advection was the primary mechanism by which the surface temperatures

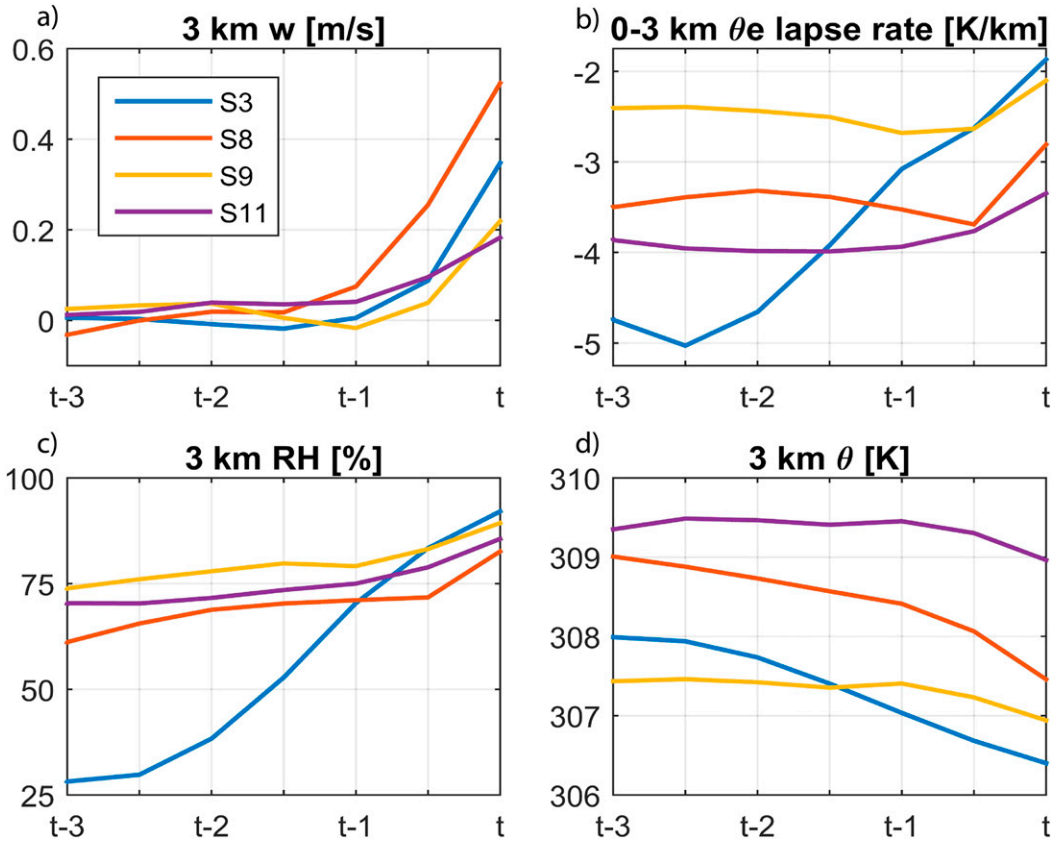


FIG. 14. Average time series of (a) vertical velocity ($m\ s^{-1}$), (b) 0–3-km equivalent potential temperature lapse rate ($K\ km^{-1}$), (c) relative humidity (%), and (d) 3-km potential temperature (K) for S3 (blue), S8 (red), S9 (gold), and S11 (purple), calculated and averaged over 3 h for all 49 points for each case, as described in section 2d, except on the 9-km grid every 30 min, and spatially smoothed using the six surrounding $x$ points and the six surrounding $y$ points for each of the 49 grid points.

increased (Fig. 12). Severe events in which surface warming contributed a relatively small amount to the total CAPE had at least some contribution from cooling aloft, reinforcing the importance of steep lapse rates in severe HSLC environments. Potential instability was likely released in multiple severe events and may be an important mechanism for rapid destabilization in some strongly forced HSLC events (Figs. 13 and 14). Shear in the low levels was also analyzed. Severe events typically had higher 0–1-km shear than nonsevere events, especially at night (Figs. 4 and 5a). However, trends in this low-level shear are rather small in comparison to the substantial changes in CAPE (Fig. 5).

Ultimately, as a result of the simulated destabilization, final/maximum CAPE was a useful ingredient for distinguishing between severe and nonsevere simulated cases, particularly when taking 0–1-km shear into consideration (e.g., Fig. 6). Given that final (just prior to convection) CAPE is a useful ingredient, but that CAPE may increase rapidly in the hours prior to the arrival of convection, forecasters must maintain situational awareness not only of the current analyzed CAPE, but also of the large-scale environmental settings in which low-CAPE values may increase very rapidly in HSLC cases.

As a result of the small sample size of severe and nonsevere events, it is difficult to determine if the results can be applied to a wide range of cases. Future work analyzing additional HSLC simulations at high spatial and temporal resolution would be beneficial to identifying characteristics of destabilization in HSLC preconvective environments. In addition, enhancement of circulations due to latent heat release from upstream convection may be extremely important in the destabilization of the environment by providing enhanced low-level flow and stronger forcing for ascent (e.g., Lackmann 2002; Mahoney and Lackmann 2007; Gold and Nielson-Gammon 2008; Schumann and Roebber 2010). This seems apt given the extremely narrow tongue of high-$\theta_e$ air advancing just ahead of and

parallel to the cold frontal convection in many cases (e.g., Fig. 7).

One of the most operationally relevant findings is that the extremely rapid destabilization occurred over periods ≤ 3 h. Therefore, utilization of 3–6-hourly model output for forecasting of severe events in low-CAPE environments may not be adequate. Also, although shear values were rather steady in time, the rapid stability changes suggest that operational mesoanalysis values of CAPE may underrepresent what will be available to convection at its time of arrival. It is encouraging that these destabilization processes can seemingly be represented in high-resolution models (as documented in section 3). Operational meteorologists would likely benefit by monitoring high-resolution model forecasts in HSLC environments for processes that indicate rapid destabilization. It would also likely be beneficial to monitor surface observations specifically for locations where surface warming will support rapidly changing SBCAPE. Given the apparent large-scale nature of the destabilization processes in this study, it would seem that identifying recurring synoptic-to-mesoscale-scale patterns could also lead to improved forecasting for these events. One recently completed study (Sherburn et al. 2016) appears to replicate the basic scenario depicted by the present model results within a much larger population of cases using a large-scale reanalysis dataset.

*Acknowledgments.* We would like to acknowledge NSF Grant AGS-1156123 and NOAA Grant NA14NWS4680013, without which this research would not have been possible. We would also like to thank all NC State collaborators as well as collaborators from the National Weather Service and Storm Prediction Center for their hard work and assistance during the CSTAR project. We are also appreciative of members of the convective storms group at NC State for their input and suggestions, as well as advisory committee member Dr. Sandra Yuter for her invaluable feedback.

## REFERENCES

Bothwell, P. D., J. A. Hart, and R. L. Thompson, 2002: An integrated three dimensional objective analysis scheme in use at the Storm Prediction Center. Preprints, *21st Conf. on Severe Local Storms/19th Conf. on Weather Analysis and Forecasting/15th Conf. on Numerical Weather Prediction*, San Antonio, TX, Amer. Meteor. Soc., JP3.1. [Available online at https://ams.confex.com/ams/pdfpapers/47482.pdf.]

Brooks, H. E., 2009: Proximity soundings for severe convection for Europe and the United States from reanalysis data. *J. Atmos. Res.*, **93**, 546–553, doi:10.1016/j.atmosres.2008.10.005.

Chen, F., and J. Dudhia, 2001: Coupling an advanced land surface–hydrology model with the Penn State–NCAR MM5 modeling system. Part I: Model description and implementation. *Mon. Wea. Rev.*, **129**, 569–585, doi:10.1175/1520-0493(2001)129<0569:CAALSH>2.0.CO;2.

Clark, M. R., 2009: The southern England tornadoes of 30 December 2006: Case study of a tornadic storm in a low CAPE, high shear environment. *J. Atmos. Res.*, **93**, 50–65, doi:10.1016/j.atmosres.2008.10.008.

——, 2013: A provisional climatology of cool-season convective lines in the UK. *J. Atmos. Res.*, **123**, 180–196, doi:10.1016/j.atmosres.2012.09.018.

Cohen, A. E., S. M. Cavallo, M. C. Coniglio, and H. E. Brooks, 2015: A review of planetary boundary layer parameterization schemes and their sensitivity in simulating southeastern U.S. cold season severe weather environments. *Wea. Forecasting*, **30**, 591–612, doi:10.1175/WAF-D-14-00105.1.

Coleman, T. A., and P. G. Dixon, 2014: An objective analysis of tornado risk in the United States. *Wea. Forecasting*, **29**, 366–376, doi:10.1175/WAF-D-13-00057.1.

Coniglio, M. C., H. E. Brooks, S. J. Weiss, and S. F. Corfidi, 2007: Forecasting the maintenance of quasi-linear mesoscale convective systems. *Wea. Forecasting*, **22**, 556–570, doi:10.1175/WAF1006.1.

Davis, J. M., and M. D. Parker, 2014: Radar climatology of tornadic and nontornadic vortices in high-shear, low-CAPE environments in the mid-Atlantic and southeastern United States. *Wea. Forecasting*, **29**, 828–853, doi:10.1175/WAF-D-13-00127.1.

Dial, G. L., J. P. Racy, and R. L. Thompson, 2010: Short-term convective mode evolution along synoptic boundaries. *Wea. Forecasting*, **25**, 1430–1446, doi:10.1175/2010WAF2222315.1.

Dudhia, J., 1996: A multi-layer soil temperature model for MM5. Preprints, *Sixth Mesoscale Model Users' Workshop*, Boulder, CO, PSU–NCAR, 22–24.

Evans, M., 2010: An examination of low CAPE/high shear severe convective events in the Binghamton, New York county warning area. *Natl. Wea. Dig.*, **34**, 129–144.

Gaffin, D. M., and S. S. Parker, 2006: A climatology of synoptic conditions associated with significant tornadoes across the southern Appalachian region. *Wea. Forecasting*, **21**, 735–751, doi:10.1175/WAF951.1.

Gold, D. A., and J. W. Nielson-Gammon, 2008: Potential vorticity diagnosis of the severe convective regime. Part III: The Hesston tornado outbreak. *Mon. Wea. Rev.*, **136**, 1593–1611, doi:10.1175/2007MWR2092.1.

Grams, J. S., R. L. Thompson, D. V. Snively, J. A. Prentice, G. M. Hodges, and L. J. Reames, 2012: Climatology and comparison of parameters for significant tornado events in the United States. *Wea. Forecasting*, **27**, 106–123, doi:10.1175/WAF-D-11-00008.1.

Guyer, J. L., and A. R. Dean, 2010: Tornadoes within weak CAPE environments across the continental United States. *25th Conf. on Severe Local Storms*, Denver, CO, Amer. Meteor. Soc., 1.5. [Available online at https://ams.confex.com/ams/25SLS/techprogram/paper_175725.htm.]

——, D. A. Imy, A. Kis, and K. Venable, 2006: Cool season significant (F2-F5) tornadoes in the Gulf Coast states. *23rd Conf. Severe Local Storms*, St. Louis MO, Amer. Meteor. Soc., 4.2. [Available online at https://ams.confex.com/ams/23SLS/techprogram/paper_115320.htm.]

Hobbs, P. V., J. D. Locatelli, and J. E. Martin, 1996: A new conceptual model for cyclones generated in the lee of the Rocky Mountains. *Bull. Amer. Meteor. Soc.*, **77**, 1169–1178, doi:10.1175/1520-0477(1996)077<1169:ANCMFC>2.0.CO;2.

Hong, S., and J. J. Lim, 2006: The WRF single-moment 6-class microphysics scheme (WSM6). *J. Korean Meteor. Soc.*, **42**, 129–151.

Jewett, B. F., and R. B. Wilhelmson, 2006: The role of forcing in cell morphology and evolution within midlatitude squall lines. *Mon. Wea. Rev.*, **134**, 3714–3734, doi:10.1175/MWR3164.1.

Kain, J. S., 2004: The Kain–Fritsch convective parameterization: An update. *J. Appl. Meteor.*, **43**, 170–181, doi:10.1175/1520-0450(2004)043<0170:TKCPAU>2.0.CO;2.

——, and Coauthors, 2008: Some practical considerations regarding horizontal resolution in the first generation of operational convection-allowing NWP. *Wea. Forecasting*, **23**, 931–952, doi:10.1175/WAF2007106.1.

Kirkpatrick, C., E. W. McCaul, and C. Cohen, 2011: Sensitivities of simulated convective storms to environmental CAPE. *Mon. Wea. Rev.*, **139**, 3514–3532, doi:10.1175/2011MWR3631.1.

Kis, A. K., and J. M. Straka, 2010: Nocturnal tornado climatology. *Wea. Forecasting*, **25**, 545–561, doi:10.1175/2009WAF2222294.1.

Lackmann, G. M., 2002: Cold-frontal potential vorticity maxima, the low-level jet, and moisture transport in extratropical cyclones. *Mon. Wea. Rev.*, **130**, 59–74, doi:10.1175/1520-0493(2002)130<0059:CFPVMT>2.0.CO;2.

Lane, J. D., and P. D. Moore, 2006: Observations of a non-supercell tornadic thunderstorm from Terminal Doppler Weather Radar. *23rd Conf. on Severe Local Storms*, St. Louis, MO, Amer. Meteor. Soc., P4.5. [Available online at https://ams.confex.com/ams/23SLS/techprogram/paper_115102.htm.]

Mahoney, K. M., and G. M. Lackmann, 2007: The effect of upstream convection on downstream precipitation. *Wea. Forecasting*, **22**, 255–277, doi:10.1175/WAF986.1.

McCaul, E. W., and M. L. Weisman, 1996: Simulation of shallow supercell storms in landfalling hurricane environments. *Mon. Wea. Rev.*, **124**, 408–429, doi:10.1175/1520-0493(1996)124<0408:SOSSSI>2.0.CO;2.

——, and ——, 2001: The sensitivity of simulated supercell structure and intensity to variations in the shapes of environmental buoyancy and shear profiles. *Mon. Wea. Rev.*, **129**, 664–687, doi:10.1175/1520-0493(2001)129<0664:TSOSSS>2.0.CO;2.

Mlawer, E. J., S. J. Taubman, P. D. Brown, M. J. Iacono, and S. A. Clough, 1997: RRTM, a validated correlated-k model for the longwave. *J. Geophys. Res.*, **102**, 16 663–16 682, doi:10.1029/97JD00237.

Noh, Y., W. G. Cheon, S.-Y. Hong, and S. Raasch, 2003: Improvement of the K-profile model for the planetary boundary layer based on large eddy simulation data. *Bound.-Layer Meteor.*, **107**, 401–427, doi:10.1023/A:1022146015946.

Rose, S. F., P. V. Hobbs, J. D. Locatelli, and M. T. Stoelinga, 2002: Use of a mesoscale model to forecast severe weather associated with a cold front aloft. *Wea. Forecasting*, **17**, 755–773, doi:10.1175/1520-0434(2002)017<0755:UOAMMT>2.0.CO;2.

Schneider, R. S., and A. R. Dean, 2008: A comprehensive 5-year severe storm environment climatology for the continental United States. *24th Conf. on Severe Local Storms*, Savannah, GA, Amer. Meteor. Soc., 16A.4. [Available online at https://ams.confex.com/ams/24SLS/techprogram/paper_141748.htm.]

——, ——, S. J. Weiss, and P. D. Bothwell, 2006: Analysis of estimated environments for 2004 and 2005 severe convective storm reports. *23rd Conf. on Severe Local Storms*, St. Louis, MO, Amer. Meteor. Soc., 3.5. [Available online at https://ams.confex.com/ams/23SLS/techprogram/paper_115246.htm.]

Schumacher, R. S., and R. H. Johnson, 2005: Organization and environmental properties of extreme-rain-producing mesoscale convective systems. *Mon. Wea. Rev.*, **133**, 961–976, doi:10.1175/MWR2899.1.

Schumann, M. R., and P. J. Roebber, 2010: The influence of upper-tropospheric potential vorticity on convective morphology. *Mon. Wea. Rev.*, **138**, 463–474, doi:10.1175/2009MWR3091.1.

Sherburn, K. D., and M. D. Parker, 2014: Climatology and ingredients of significant severe convection in high-shear, low-CAPE environments. *Wea. Forecasting*, **29**, 854–877, doi:10.1175/WAF-D-13-00041.1.

——, ——, J. R. King, and G. M. Lackmann, 2016: Composite environments of severe and nonsevere high-shear, low-CAPE convective events. *Wea. Forecasting*, **31**, 1899–1927, doi:10.1175/WAF-D-16-0086.1.

Skamarock, W., and Coauthors, 2008: A description of the Advanced Research WRF version 3. NCAR Tech. Note NCAR/TN-475+STR, 113 pp., doi:10.5065/D68S4MVH.

Smith, B. T., J. L. Guyer, and A. R. Dean, 2008: The climatology, convective mode, and mesoscale environment of cool season severe thunderstorms in the Ohio and Tennessee valleys, 1995-2006. *24th Conf. on Severe Local Storms,* Savannah, GA, Amer. Meteor. Soc., 13B.7. [Available online at https://ams.confex.com/ams/24SLS/techprogram/paper_141968.htm.]

——, R. L. Thompson, J. S. Grams, C. Broyles, and H. E. Brooks, 2012: Convective modes for significant severe thunderstorms in the contiguous United States. Part I: Storm classification and climatology. *Wea. Forecasting*, **27**, 1114–1135, doi:10.1175/WAF-D-11-00115.1.

Thompson, R. L., R. Edwards, J. A. Hart, K. L. Elmore, and P. Markowski, 2003: Close proximity soundings within supercell environments obtained from the Rapid Update Cycle. *Wea. Forecasting*, **18**, 1243–1261, doi:10.1175/1520-0434(2003)018<1243:CPSWSE>2.0.CO;2.

——, J. S. Grams, and J. A. Prentice, 2008: Synoptic environments and convective modes associated with significant tornadoes in the contiguous United States. *24th Conf. on Severe Local Storms*, Savannah, GA, Amer. Meteor. Soc., 16A.3. [Available online at https://ams.confex.com/ams/24SLS/techprogram/paper_142210.htm.]

Tochimoto, E., and H. Niino, 2016: Structural and environmental characteristics of extratropical cyclones that cause tornado outbreaks in the warm sector: A composite study. *Mon. Wea. Rev.*, **144**, 945–969, doi:10.1175/MWR-D-15-0015.1.

Trier, S. B., C. A. Davis, D. Ahijevych, M. L. Weisman, and G. H. Bryan, 2006: Mechanisms supporting long-lived episodes of propagating nocturnal convection within a 7-day WRF model simulation. *J. Atmos. Sci.*, **63**, 2437–2461, doi:10.1175/JAS3768.1.

Wheatley, D. M., and R. J. Trapp, 2008: The effect of mesoscale heterogeneity on the genesis and structure of mesovortices within quasi-linear convective systems. *Mon. Wea. Rev.*, **136**, 4220–4241, doi:10.1175/2008MWR2294.1.